Deciphering stable water isotope records of firn cores from a strongly maritime, high-accumulation site on the Antarctic Peninsula

Kirstin Hoffmann-Abdi[1,2*], Hanno Meyer[1], Francisco Fernandoy[3], Johannes Freitag[4], Fyntan M. Shaw[1], Martin Werner[4], Elizabeth R. Thomas[5], Joseph R. McConnell[6] and Christoph Schneider[2]

[1]Alfred Wegener Institute, Helmholtz Centre for Polar and Marine Research, Research Unit Potsdam, Telegrafenberg A45, Potsdam, 14473, Germany; Kirstin.Hoffmann@awi.de; Hanno.Meyer@awi.de; Fyntan.Shaw@awi.de

[2]Geography Department, Humboldt-Universität zu Berlin, Unter den Linden 6, Berlin, 10099, Germany; hofmanki@hu-berlin.de; christoph.schneider@geo.hu-berlin.de

[3]Facultad de Ingeniería, Universidad Nacional Andrés Bello, Viña del Mar, 2531015, Chile; francisco.fernandoy@unab.cl

[4]Alfred Wegener Institute, Helmholtz Centre for Polar and Marine Research, Am Alten Hafen 26, Bremerhaven, 27568, Germany; Johannes.Freitag@awi.de; Martin.Werner@awi.de

[5]Ice Dynamics and Paleoclimate, British Antarctic Survey, High Cross, Madingley Road, Cambridge, CB3 0ET, UK; lith@bas.ac.uk

[6]Division of Hydrologic Sciences, Desert Research Institute, 2215 Raggio Parkway, Reno, NV 89512, USA; Joe.McConnell@dri.edu

*****Correspondence: Kirstin.Hoffmann@awi.de

Supplementary Materials

Method S1. Dating of firn core OH-9

Hydrogen peroxide (H_2O_2) is a suitable parameter for dating of firn cores from the northern Antarctic Peninsula (AP), since the high accumulation rates prevent its fast dissipation from the snowpack after deposition (Sigg and Neftel, 1988; Frey and others, 2006; Travassos and others, 2021). It is produced in the atmosphere through photochemical reactions under the influence of solar UV radiation and water vapor (Lee and others, 2000). Therefore, H_2O_2 typically exhibits a clear seasonality following cyclic changes in solar radiation and air temperature (McConnell and others, 1997; Riedel and others, 2000). When washed out of the atmosphere by precipitation, it reaches the Earth's surface through wet deposition and accumulates in the snowpack (Sigg and Neftel, 1988; Riedel and others, 2000). If not affected by post-depositional processes (e.g., degassing from the snowpack, relocation due to meltwater

percolation) the highest H_2O_2 peak in each annual cycle most likely represents the time around the summer solstice and the minimum the time around the winter solstice (Riedel and others, 2000; Steig and others, 2005). Here we used the H_2O_2 summer maxima for annual layer counting (ALC) since the clear identification of the winter minima in the highly resolved record is difficult.

The drill date of OH-9 (28th January 2014) was used as uppermost tie point for constructing the age model. As previously observed for OH-12 (Hoffmann-Abdi and others, 2021), the H_2O_2 profile of OH-9 shows seasonal cycles with the uppermost summer maximum (~ 0.5 m depth) exhibiting a double peak. In the bottom part of the core, i.e., below 10 m depth, the seasonality is less clear. Following the dating procedure applied to OH-12 (Hoffmann-Abdi and others, 2021), we assigned 1st January 2014 to the first maximum (from the top) of the H_2O_2 double peak at about 0.5 m depth, as the latter had already formed at the time of core drilling (end of January 2014; Table 1 in the main text). 1st January 2013 was set to the well-defined maximum at about 6.2 m depth. For the third year identified below 10 m depth (2012), the first (from the top) clearly pronounced maximum peak at about 10.2 m depth was set to 1st January, as it is almost three times higher than the record mean of 56 ppb (cf. Hoffmann-Abdi and others, 2021).

The results of ALC applied to the H_2O_2 profile were confirmed with measurements of methane sulfonic acid (MSA) which shows the clearest seasonal behaviour among the measured ions (Fig. 2a in the main text). MSA is a photooxidation product of dimethylsulfide (DMS), which in turn is produced by marine phytoplankton with greatest fluxes occurring in the marginal sea ice zone (Abram and others, 2013; Osman and others, 2017). Atmospheric MSA concentrations rapidly decrease with increasing altitude and distance from the source. At coastal sites they exhibit a distinct maximum during the late spring to summer months (Abram and others, 2013; Osman and others, 2017). The H_2O_2 maximum of the first and third year, respectively, has a corresponding maximum in the MSA record, whereas the second year lacks a distinct MSA peak (Fig. 2a in the main text).

The age scale was then derived by linear interpolation between two consecutive tie points and below 10 m depth by linear extrapolation using the depth-age-relationship between the clearly identifiable peaks of 2013 and 2014. According to the ALC-dating, OH-9 spans two full years, 2012 and 2013, confirming the suggestion of Hoffmann-Abdi and others (2021), that the age model previously derived by Fernandoy and others (2018) has a dating error of +1 year.

To estimate the dating uncertainty of the derived age model, we calculated age models for different cases of identifying January peaks in the H_2O_2 record and determined the mean

temporal offset between them. For example, we assumed that January 1st equals the second maximum (from the top) of the double peak at about 0.5 m depth or the minimum between the two peaks, which could simply have been caused by missing snow precipitation and/or higher air temperatures (McConnell and others, 1997; McConnell and others, 1998). We did not consider assigning January 1st to the secondary maxima at about 1.5-2 m and 6.5-7 m depth (Fig. 2a in the main text), which also exhibit double peaks. Taking into account the strong linkage of H_2O_2 to the annual insolation cycle, the drill date of the core (end of January) and an average accumulation rate of 2500 kg m^{-2} a^{-1} at the study site (Hoffmann-Abdi and others, 2021), it is more likely that these maxima were formed at the beginning of the sunlit period in austral spring rather than at the beginning of the calendar year (January). Below 10 m depth, the H_2O_2 record is likely biased due to melt water percolation, as proposed by Hoffmann-Abdi and others (2021) for core OH-12 in a section covering the same time interval (2011/2012). Consequently, 1st January 2012 could in principle be assigned to any of the H_2O_2 peaks in the bottom part of OH-9, regardless of its height. Hence, the described procedure resulted in a dating uncertainty of ± 1 month in the upper part (≤ 10 m) and ± 5 months in the lower part (> 10 m) of the core.

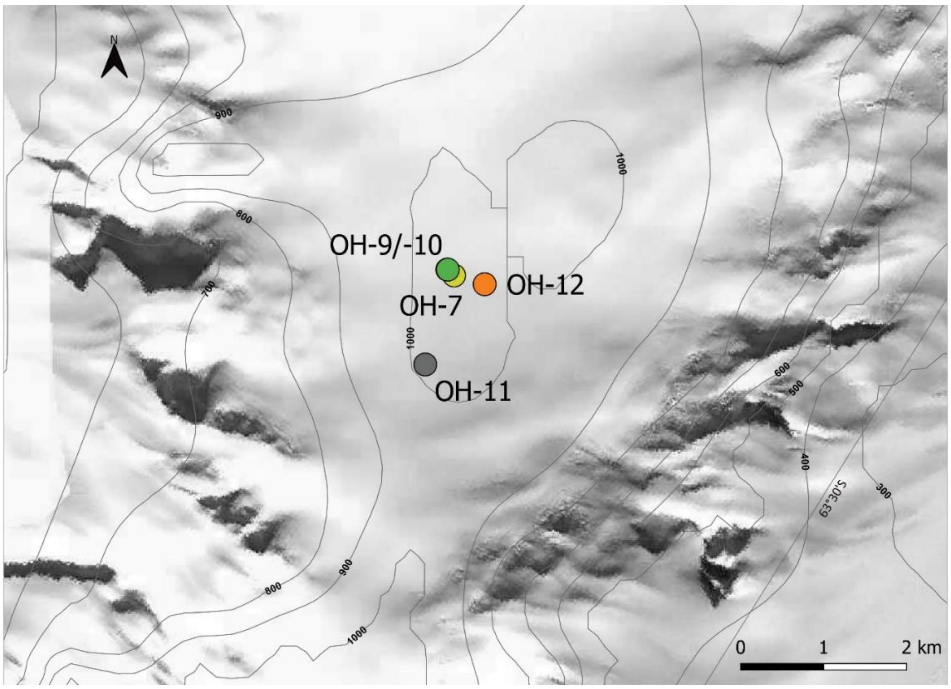

Figure S1. Detailed map of the study site on Plateau Laclavere (LCL), northern Antarctic Peninsula, showing the location of the drill sites of firn cores OH-7, OH-9, OH-10, OH-11 and OH-12.

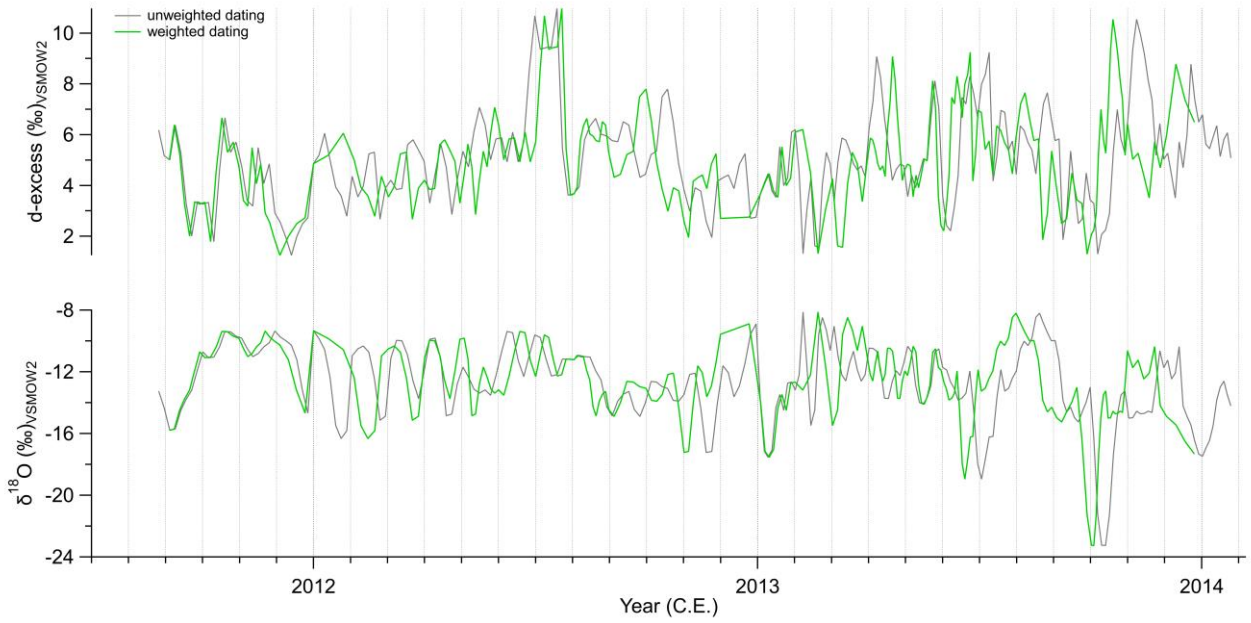

Figure S2. Comparison of the weighted age scale of firn core OH-9 (green) with the ALC-based (unweighted) age scale (grey). The maximum offset between both age scales is 28 days.

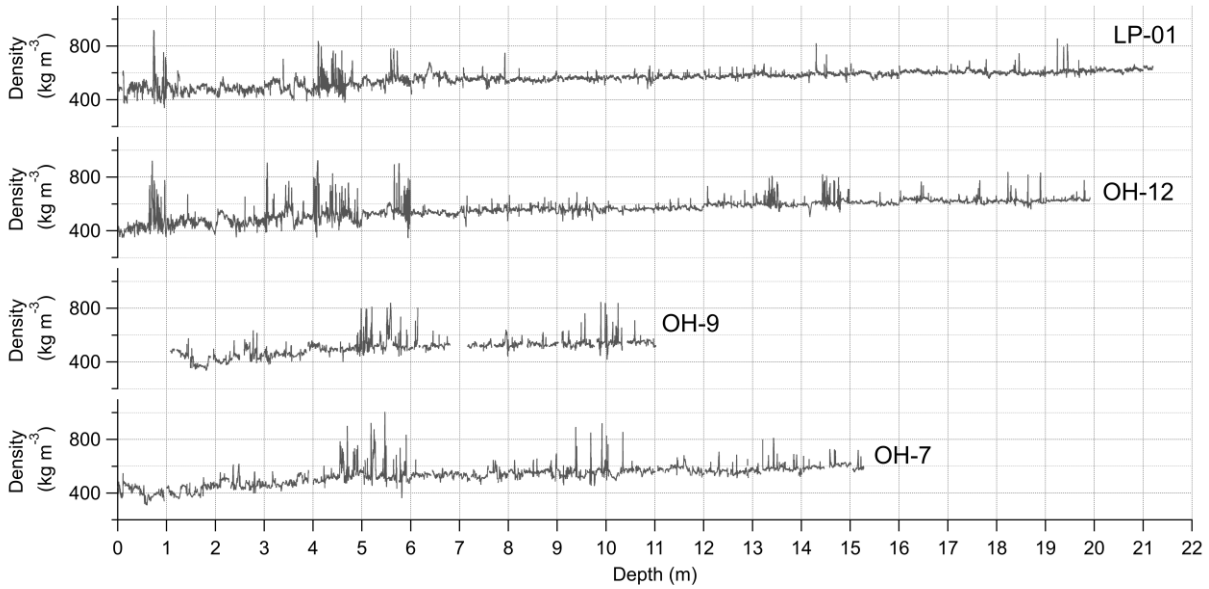

Figure S3. High-resolution density profiles of firn cores OH-7, OH-9, OH-12 and LP-01. The snow-firn-density transition (550 kg m^{-3}) estimated by linear regression across the entire density-depth profile is at about 9.2 m depth for OH-7, at about 9.3 m depth for OH-9, at about 8.4 m depth for OH-12 and at about 8.9 m depth for LP-01, respectively.

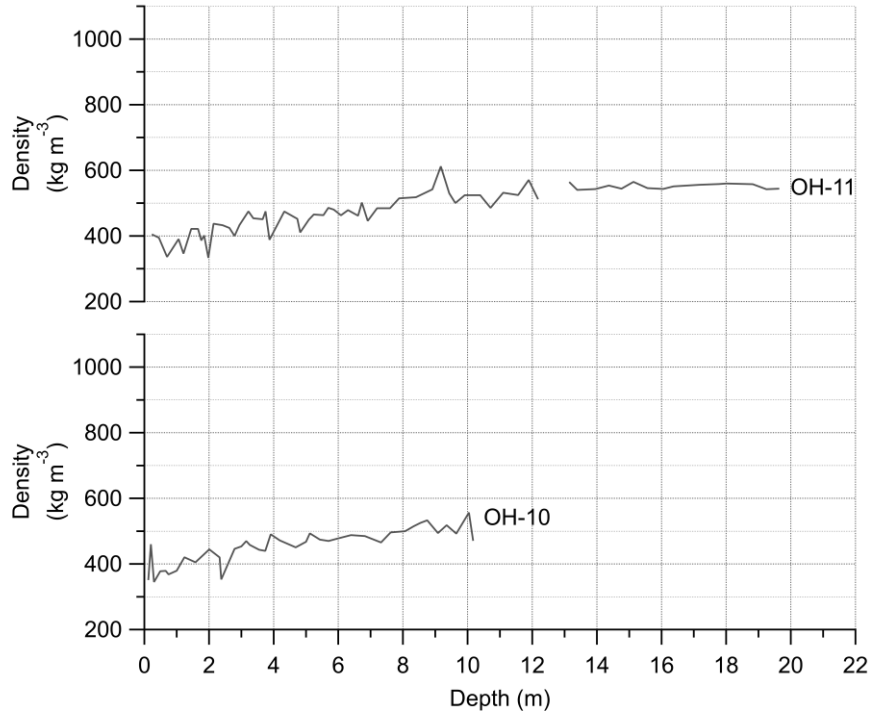

Figure S4. Density profiles of firn cores OH-10 and OH-11.

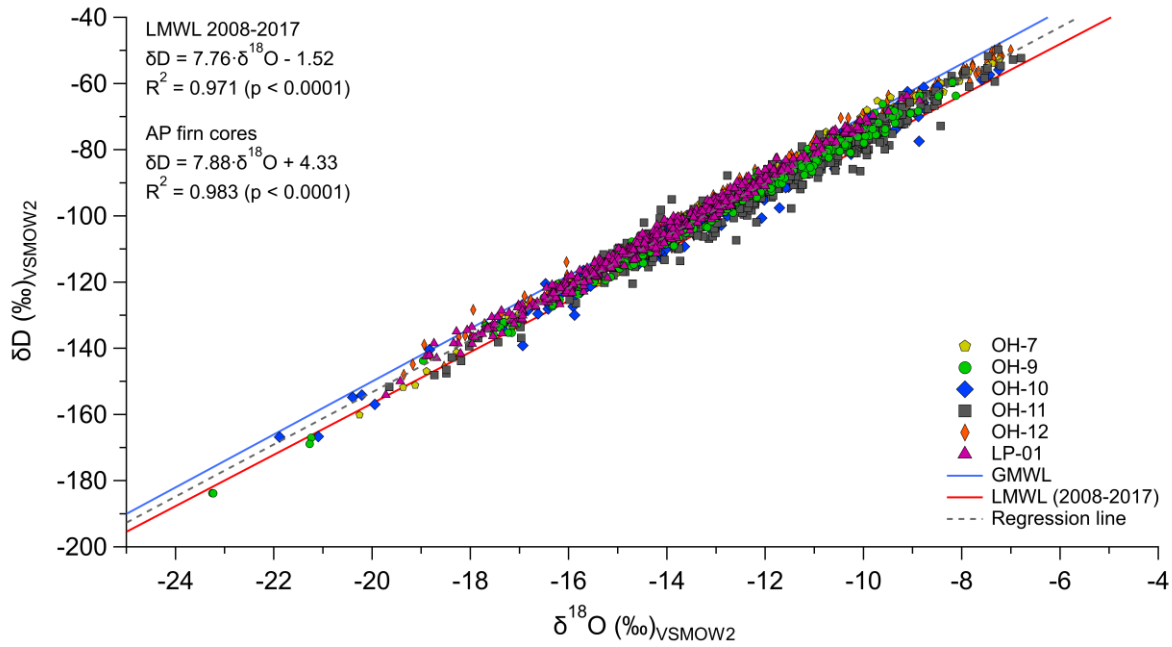

Figure S5. $\delta^{18}O$-δD-relationship of the six firn cores of Table 1 in the main text. The equation and coefficient of determination (R^2) of the linear regression considering all firn core samples (n = 1982; grey dashed line) is also given. The Global Meteoric Water Line (GMWL) is indicated in blue. The Local Meteoric Water Line (LMWL) for the study site (red) with its equation and R^2 is from Hoffmann-Abdi and others (2021).

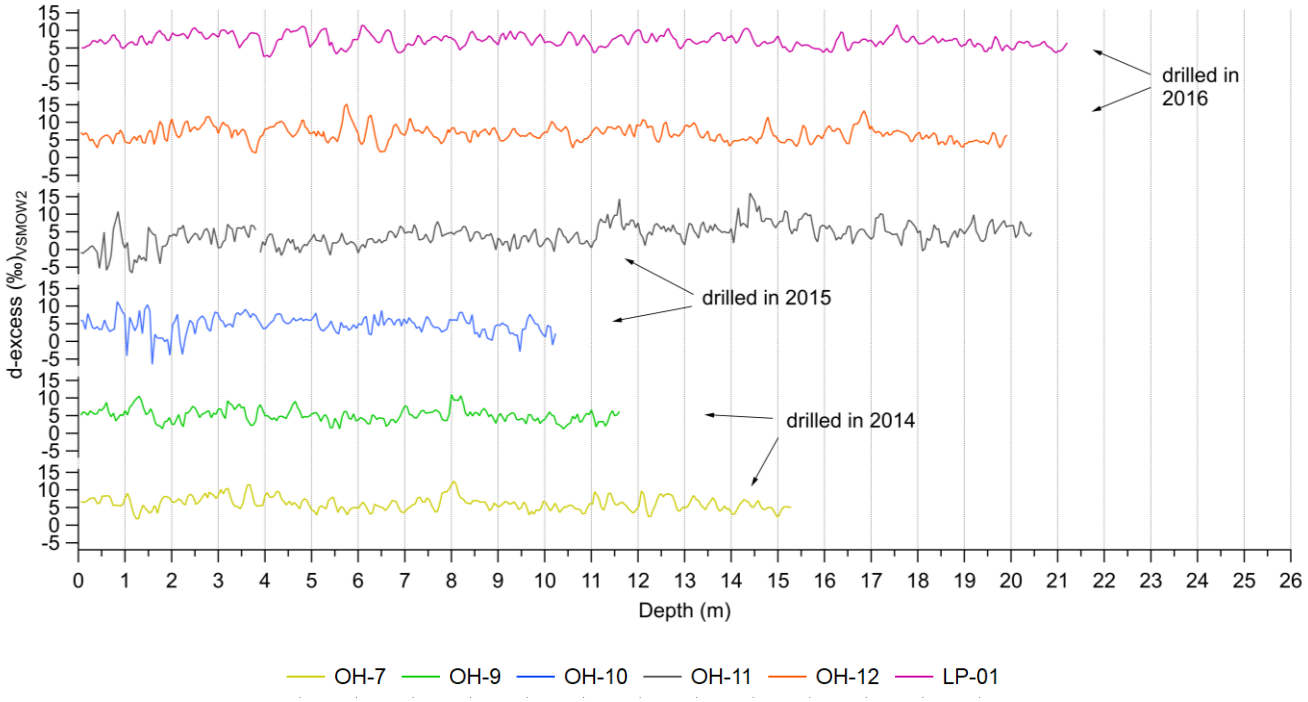

Figure S6. D-excess profiles of the six firn cores of Table 1 in the main text with the year of drilling indicated.

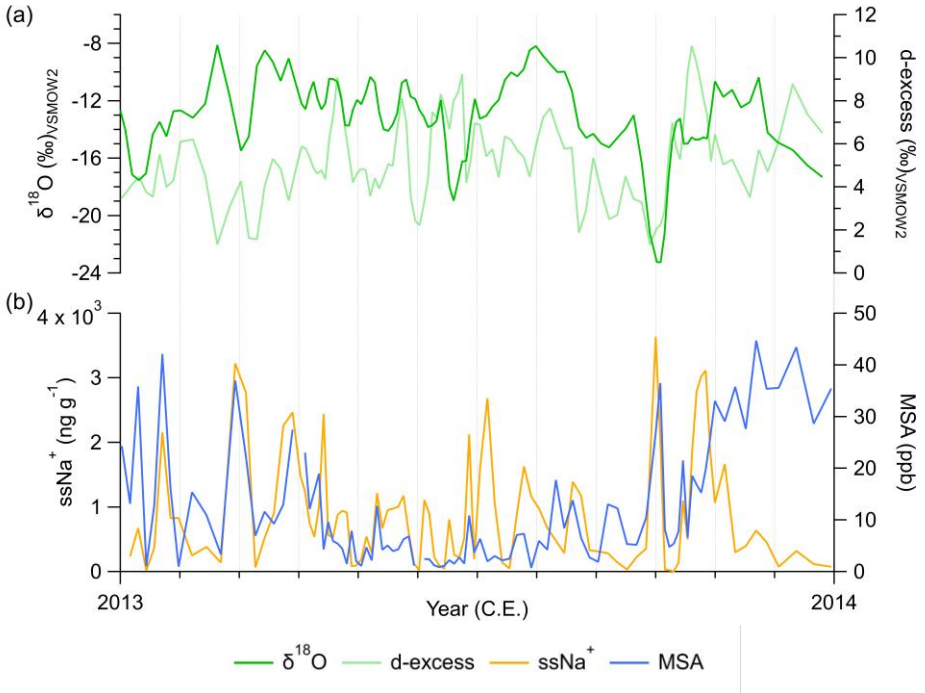

Figure S7. Time series of (a) $\delta^{18}O$ (green) and d-excess (light green) of firn core OH-9 compared to OH-9 records of (b) sea-salt sodium ($ssNa^+$; dark yellow) and MSA (blue) for the year 2013.

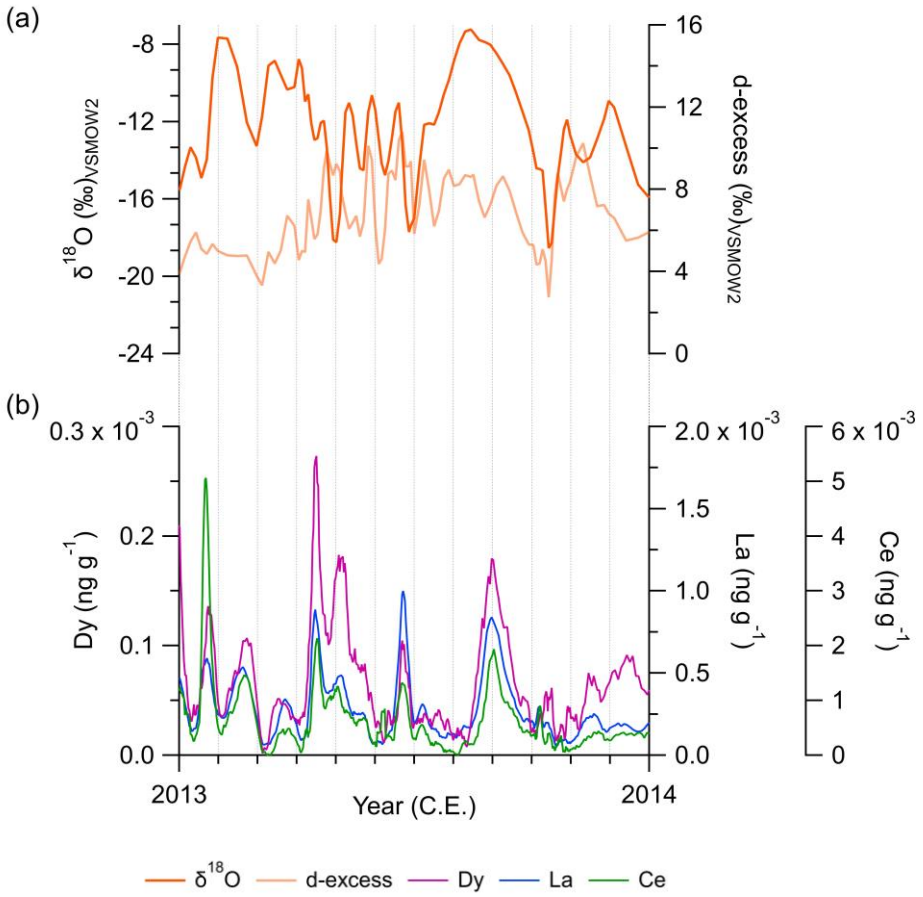

Figure S8. Time series of (a) $\delta^{18}O$ (orange) and d-excess (light orange) of firn core OH-12 compared to OH-12 records of (b) dysprosium (Dy; magenta), lanthanum (La; blue) and cerium (Ce; green) for the year 2013.

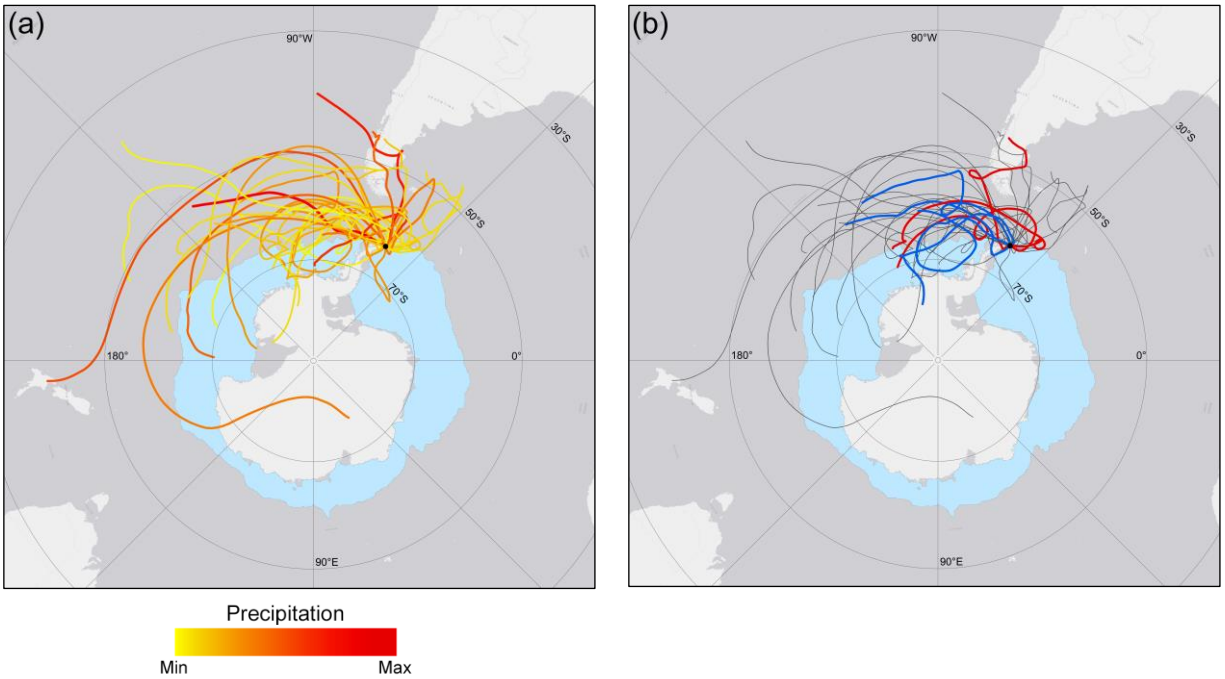

Figure S9. Five-day backward trajectories calculated for days with precipitation (≥ 1mm) registered at Bernardo O'Higgins (OH) and Esperanza (EP) stations in the period covered by the sequence of $\delta^{18}O$ minima and maxima preceding the MMM-pattern (May-June 2013). In (a) trajectories were ranked according to the amount of precipitation delivered, and then color-coded from yellow (lowest rank) to red (highest rank). For days on which precipitation was recorded at both OH and EP stations, the higher precipitation amount was used for the ranking. The thickness of the trajectories increases as the amount of precipitation increases. In (b) trajectories directly related to the $\delta^{18}O$ maxima are marked in red and those related to the $\delta^{18}O$ minima in blue. In (a) and (b) the mean monthly sea-ice extent for June 2013 is shown in blue shading. The black dot indicates the location of the drill site of firn core OH-12 used as initial point for backward trajectory modelling.

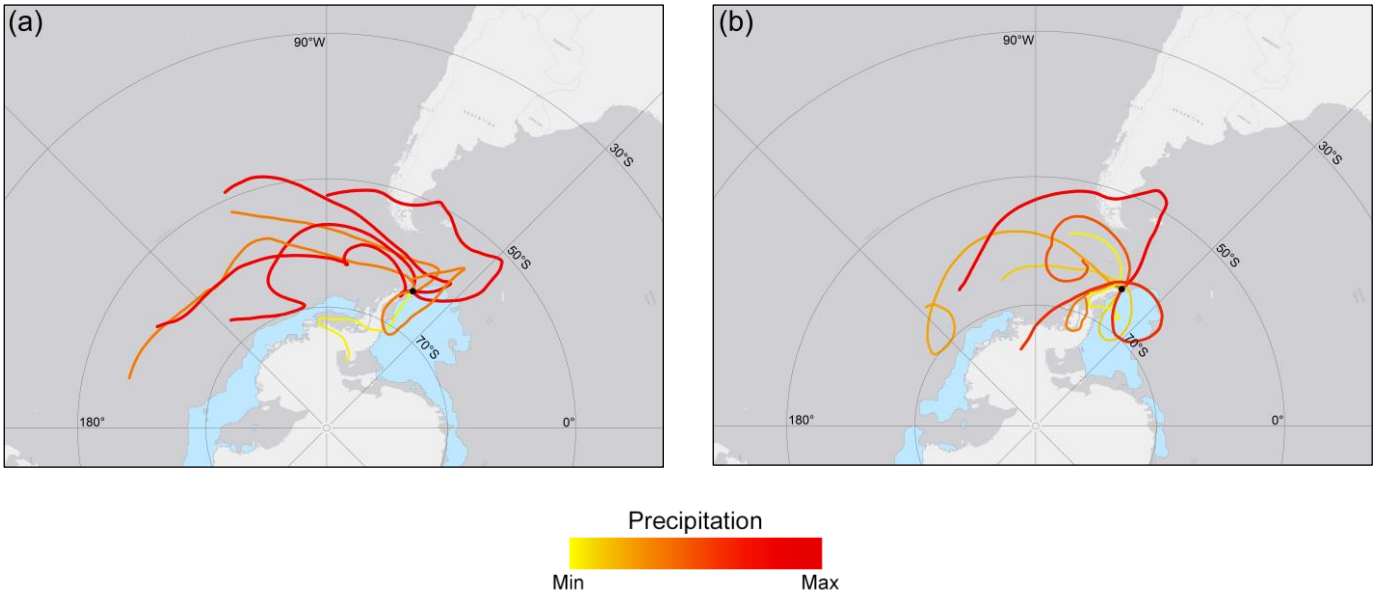

Figure S10. Five-day backward trajectories calculated for days with precipitation (≥ 1mm) registered at Bernardo O'Higgins (OH) and Esperanza (EP) stations in (a) January 2013 and (b) February 2013. Trajectories were ranked according to the amount of precipitation delivered, and then color-coded from yellow (lowest rank) to red (highest rank). For days on which precipitation was recorded at both OH and EP stations, the higher precipitation amount was used for the ranking. The thickness of the trajectories increases as the amount of precipitation increases. The mean monthly sea-ice extent for January and February 2013 is shown in blue shading. The black dot in (a) and (b) indicates the location of the drill site of firn core OH-12 used as initial point for backward trajectory modelling.

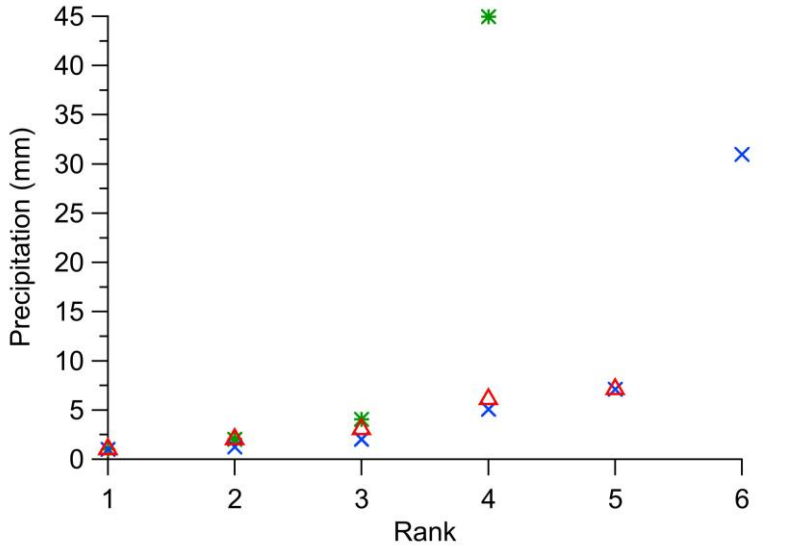

Figure S11. Ranking of precipitation amounts delivered to the northern Antarctic Peninsula by calculated five-day backward trajectories at around the time of the three extrema of the $\delta^{18}O$ MMM-pattern (green asterisks: Minimum in June/July 2013; red triangles: Maximum in August 2013; blue crosses: Minimum in October 2013).

Table S1. Coordinates and altitude of the geographic location for the Antarctic stations Bernardo O'Higgins (OH), Bellingshausen (BH) and Esperanza (EP) as well as for the ERA5 and ECHAM6-wiso grid points closest to the OH-12 drill site on LCL.

Station/Grid point	OH	BH	EP	ERA5	ECHAM6-wiso
Coordinates	63°19'15.42" S 57°53'59.21" W	62°11'53.46" S 58°57'38.19" W	63°23'49.05" S 56°59'52.99" W	63°37'30" S 57°52'30" W	63°6'59.4" S 58°7'30" W
Altitude (m a.s.l.)	12	16	25	270	130

Table S2. Overview of physical, isotope-geochemical and glacio-chemical parameters available for the six firn cores of Table 1 in the main text.

Firn core/ Parameter	physical	isotope-geochemical	glacio-chemical
OH-7	density (high resolution)	$\delta^{18}O$, δD, d-excess	-
OH-9	density (high resolution)	$\delta^{18}O$, δD, d-excess	Cl^-, Br^-, F^-, NO_3^-, SO_4^{2-}, Na^+, K^+, Mg^{2+}, Ca^{2+}, MSA, H_2O_2, conductivity
OH-10	density	$\delta^{18}O$, δD, d-excess	-
OH-11	density	$\delta^{18}O$, δD, d-excess	-
OH-12	density (high resolution)	$\delta^{18}O$, δD, d-excess	Br^-, Cl^-, I^-, Na^+, Mg^{2+}, Ca^{2+}, Sr^{2+}, Rb^+, Al^{3+}, S, Bi, Mn, Zn, Fe, P, Pb, Cd, La, Ce, Dy, Tl, U, H_2O_2, HNO_3, NH_4^+, black carbon (BC), insoluble particles, conductivity
LP-01	density (high resolution)	$\delta^{18}O$, δD, d-excess	-

Table S3. Results of cross-correlation analysis for the non-depth-aligned and depth-aligned high-resolution density records (10 cm means) of firn cores OH-7, OH-9, OH-12 and LP-01. Cross-correlations for non-depth-aligned density records are only calculated between cores drilled in the same year (OH-7 and OH-9; OH-12 and LP-01). All correlations are statistically significant ($p < 0.05$, $\alpha = 0.05$). Details on the depth alignment are given in the main text.

	Non-depth-aligned records				Depth-aligned records			
Firn core	OH-7	OH-9	OH-12	LP-01	OH-7	OH-9	OH-12	LP-01
OH-7								
r	1	0.65	-	-	1	0.75	0.76	0.74
p	0	< 0.0001	-	-	0	< 0.0001	< 0.0001	< 0.0001
OH-9								
r		1	-	-		1	0.74	0.66
p		0	-	-		0	< 0.0001	< 0.0001
OH-12								
r			1.0	0.84			1	0.84
p			0	< 0.0001			0	< 0.0001
LP-01								
r				1				1
p				0				0

Table S4. Results of cross-correlation analysis for depth-aligned stable water isotope records (10 cm means) of the six firn cores of Table 1 in the main text with respect to the depth-interval from 9.8 m to 14.6 m, corresponding to the year 2013 in OH-12. Statistically significant correlations ($p < 0.05$, $\alpha = 0.05$) that are higher than the mean cross-correlation ($\delta^{18}O$: 0.531; δD: 0.534; d-excess: 0.294; Table S5) are marked in bold blue and those that are lower than the mean cross-correlation in bold red.

Firn core	OH-7			OH-9			OH-10			OH-11			OH-12			LP-01		
	$\delta^{18}O$	δD	d-excess	$\delta^{18}O$	δD	d-excess	$\delta^{18}O$	δD	d-excess	$\delta^{18}O$	δD	d-excess	$\delta^{18}O$	δD	d-excess	$\delta^{18}O$	δD	d-excess
OH-7																		
r	1	1	1	**0.67**	**0.68**	**0.36**	**0.45**	**0.48**	**0.33**	**0.37**	**0.40**	**0.51**	**0.50**	**0.53**	**0.36**	**0.43**	**0.42**	0.24
p	0	0	0	< 0.0001	< 0.0001	< 0.05	< 0.01	< 0.001	< 0.05	< 0.05	< 0.01	< 0.001	< 0.001	< 0.001	< 0.05	< 0.01	< 0.01	< 0.10
OH-9																		
r				1	1	1	**0.47**	**0.48**	0.09	**0.52**	**0.53**	-0.07	**0.52**	**0.53**	**0.39**	**0.45**	**0.46**	**0.29**
p				0	0	0	< 0.001	< 0.001	0.52	< 0.001	< 0.001	0.65	< 0.001	< 0.001	< 0.01	< 0.01	< 0.01	< 0.05
OH-10																		
r							1	1	1	**0.61**	**0.62**	**0.35**	**0.70**	**0.69**	**0.50**	**0.68**	**0.65**	0.20
p							0	0	0	< 0.0001	< 0.0001	< 0.05	< 0.0001	< 0.0001	< 0.001	< 0.0001	< 0.0001	0.17
OH-11																		
r										1	1	1	**0.42**	**0.41**	**0.26**	**0.50**	**0.48**	0.12
p										0	0	0	< 0.01	< 0.01	< 0.1	< 0.001	< 0.001	0.41
OH-12																		
r													1	1	1	**0.67**	**0.66**	**0.45**
p													0	0	0	< 0.0001	< 0.0001	< 0.01
LP-01																		
r																1	1	1
p																0	0	0

Table S5. Mean cross-correlations and signal-to-noise ratios for depth-aligned stable water isotope records (10 cm means) of the six firn cores of Table 1 in the main text for different depth intervals. The depth intervals 10.2-12.5 m and 9.8-14.6 m correspond to the 2013 MMM-pattern and the entire year 2013 in firn core OH-12, respectively.

	$\delta^{18}O$	δD	d-excess
Depth interval: 10.2-12.5 m (MMM-pattern)			
Mean cross-correlation	0.733	0.734	0.447
Signal-to-noise ratio	2.75	2.76	0.81
Depth interval: 9.8-14.6 m (2013)			
Mean cross-correlation	0.531	0.534	0.294
Signal-to-noise ratio	1.13	1.15	0.42
Common depth interval between two cores (multiannual scale)			
Mean cross-correlation	0.377	0.381	0.177
Signal-to-noise ratio	0.61	0.62	0.22

Table S6. Correlations between stable water isotope time series of firn core OH-12 and near-surface air temperature records from close-by Antarctic stations (Bernardo O'Higgins [OH], Bellingshausen [BH] and Esperanza [EP]) and ERA5 reanalysis data, calculated for the year 2013 based on monthly means. ERA5 reanalysis data were extracted from the grid point closest to the OH-12 drill site and were corrected for the difference in elevation as described in the main text. Statistically significant correlations ($p < 0.05$, $\alpha = 0.05$) are marked in bold.

Temperature record	OH	BH	EP	ERA5
$\delta^{18}O$				
r	-0.14	-0.25	0.04	0.03
p	0.65	0.43	0.90	0.93
δD				
r	-0.21	-0.31	-0.02	-0.03
p	0.52	0.32	0.95	0.92
d-excess				
r	**-0.75**	**-0.73**	**-0.74**	**-0.78**
p	< 0.01	< 0.01	< 0.01	< 0.01

Table S7. Results of cross-correlation analysis for the depth-aligned isotopic records (10 cm means) of the six firn cores of Table 1 in the main text with respect to the common depth interval between two cores. No statistically significant correlations exist for the non-depth-aligned isotopic records. For $\delta^{18}O$ and δD all correlations are statistically significant ($p < 0.05$, $\alpha = 0.05$), for the d-excess statistically significant correlations are marked in bold. Details on the depth alignment are given in the main text.

$\delta^{18}O$	OH-7	OH-9	OH-10	OH-11	OH-12	LP-01
OH-7	1 0	0.57 < 0.0001	0.47 < 0.001	0.24 < 0.01	0.42 < 0.0001	0.35 < 0.001
OH-9		1 0	0.41 < 0.001	0.26 < 0.01	0.39 < 0.0001	0.28 < 0.01
OH-10			1 0	0.41 < 0.0001	0.42 < 0.0001	0.41 < 0.0001
OH-11				1 0	0.32 < 0.0001	0.27 < 0.001
OH-12					1 0	0.45 < 0.0001
LP-01						1 0
δD						
OH-7	1 0	0.52 < 0.0001	0.49 < 0.0001	0.28 < 0.001	0.43 < 0.0001	0.33 < 0.001
OH-9		1 0	0.40 < 0.001	0.32 < 0.001	0.39 < 0.0001	0.29 < 0.01
OH-10			1 0	0.40 < 0.0001	0.40 < 0.0001	0.39 < 0.0001
OH-11				1 0	0.32 < 0.0001	0.27 < 0.001
OH-12					1 0	0.43 < 0.0001
LP-01						1 0
d-excess						
OH-7	1 0	**0.25** < 0.01	**0.40** < 0.01	0.03 0.73	**0.37** < 0.001	**0.25** < 0.01
OH-9		1 0	0.15 0.25	-0.19 0.04	**0.34** < 0.001	**0.43** < 0.0001
OH-10			1 0	-0.04 0.72	**0.21** < 0.05	**0.24** < 0.05
OH-11				1 0	-0.05 0.56	-0.12 0.12
OH-12					1 0	**0.37** < 0.0001
LP-01						1 0

Table S8. Results of cross-correlation analysis between stable water isotopes and sea salt indicators of firn cores OH-9 and OH-12 (10 cm means) with respect to the depth-interval from 10.2 m to 12.5 m, corresponding to the period of the 2013 MMM-pattern. For OH-9 the correlations of stable water isotopes with MSA are also given. Statistically significant correlations ($p < 0.05$, $\alpha = 0.05$) are marked in bold.

		OH-9			OH-12		
		$\delta^{18}O$	δD	d-excess	$\delta^{18}O$	δD	d-excess
$ssNa^+$							
	r	-0.13	-0.14	-0.26	-0.33	-0.32	0.08
	p	0.56	0.52	0.22	0.12	0.14	0.72
Cl^-							
	r	-0.12	-0.13	-0.27	-0.35	-0.34	0.05
	p	0.59	0.54	0.22	< 0.10	0.11	0.82
Ca^{2+}							
	r	-0.20	-0.23	**-0.50**	-0.37	-0.35	0.09
	p	0.37	0.30	< 0.05	< 0.10	< 0.10	0.69
Sr^{2+}							
	r	-	-	-	**-0.42**	-0.41	-0.01
	p	-	-	-	< 0.05	< 0.10	0.96
MSA							
	r	**-0.47**	**-0.49**	**-0.51**	-	-	-
	p	< 0.05	< 0.05	< 0.05	-	-	-

References

Abram, N.J., E.W. Wolff and M.A. Curran. 2013. A review of sea ice proxy information from polar ice cores. *Quaternary Science Reviews*, **79**, 168–183. doi: 10.1016/j.quascirev.2013.01.011.

Fernandoy, F., D. Tetzner, H. Meyer, G. Gacitúa, K. Hoffmann, U. Falk, F. Lambert and S. MacDonell. 2018. New insights into the use of stable water isotopes at the northern Antarctic Peninsula as a tool for regional climate studies. *The Cryosphere*, **12**(3), 1069–1090. doi: 10.5194/tc-12-1069-2018.

Frey, M.M., R.C. Bales and J.R. McConnell. 2006. Climate sensitivity of the century-scale hydrogen peroxide (H2O2) record preserved in 23 ice cores from West Antarctica. *Journal of Geophysical Research*, **111**(D21). doi: 10.1029/2005JD006816.

Hoffmann-Abdi, K., F. Fernandoy, H. Meyer, J. Freitag, T. Opel, J.R. McConnell and C. Schneider. 2021. Short-Term Meteorological and Environmental Signals Recorded in a Firn Core from a High-Accumulation Site on Plateau Laclavere, Antarctic Peninsula. *Geosciences*, **11**(10), 428. doi: 10.3390/geosciences11100428.

Lee, M., B.G. Heikes and D.W. O'Sullivan. 2000. Hydrogen peroxide and organic hydroperoxide in the troposphere: a review. *Atmospheric Environment*, **34**(21), 3475–3494. doi: 10.1016/s1352-2310(99)00432-x.

McConnell, J.R., R.C. Bales, R.W. Stewart, A.M. Thompson, M.R. Albert and R. Ramos. 1998. Physically based modeling of atmosphere-to-snow-to-firn transfer of H2O2 at South Pole. *Journal of Geophysical Research*, **103**(D9), 10561–10570. doi: 10.1029/98JD00460.

McConnell, J.R., J.R. Winterle, R.C. Bales, A.M. Thompson and R.W. Stewart. 1997. Physically based inversion of surface snow concentrations of H2O2 to atmospheric concentrations at South Pole. *Geophysical Research Letters*, **24**(4), 441–444. doi: 10.1029/97GL00183.

Osman, M., S.B. Das, O. Marchal and M.J. Evans. 2017. Methanesulfonic acid (MSA) migration in polar ice: data synthesis and theory. *The Cryosphere*, **11**(6), 2439–2462. doi: 10.5194/tc-11-2439-2017.

Riedel, K., R. Weller, O. Schrems and G. König-Langlo. 2000. Variability of tropospheric hydroperoxides at a coastal surface site in Antarctica. *Atmospheric Environment*, **34**(29-30), 5225–5234. doi: 10.1016/S1352-2310(00)00322-8.

Sigg, A. and A. Neftel. 1988. Seasonal Variations in Hydrogen Peroxide in Polar Ice Cores. *Annals of Glaciology*, **10**, 157–162. doi: 10.3189/S0260305500004353.

Steig, E.J., P.A. Mayewski, D.A. Dixon, S.D. Kaspari, M.M. Frey, D.P. Schneider, S.A. Arcone, G.S. Hamilton, V. Blue Spikes, M. Albert, D. Meese, A.J. Gow, C.A. Shuman, J.W. White, S. Sneed, J. Flaherty and M. Wumkes. 2005. High-resolution ice cores from US ITASE (West Antarctica): development and validation of chronologies and determination of precision and accuracy. *Annals of Glaciology*, **41**, 77–84. doi: 10.3189/172756405781813311.

Travassos, J.M., S.S. Martins, M. Potocki and J.C. Simões. 2021. Reconstruction of annual accumulation rate on firn, synchronising H_2O_2 concentration data with an estimated temperature record. *The Cryosphere*, **15**(7), 3495–3505. doi: 10.5194/tc-15-3495-2021.